 CMC, vol.11, no.1, pp.59-77, 2009

A Three-Dimensional Meshless Scheme with Background Grid for Electrostatic-Structural Analysis

Ming-Hsiao Lee and Wen-Hwa Chen

Abstract: On the analysis of electrostatic-structural coupled problems as encountered in many electrostatic driven MEMS devices, the electrostatic analysis domain is often extremely distorted due to the deflection of the structure. This kind of problem is difficult to be dealt with by almost all kinds of available numerical methods. A new three-dimensional meshless scheme with background grid is thus proposed herein. By this scheme, a three-dimensional fixed background grid with regularly-distributed nodes is utilized. Another set of discretized boundary grid is employed to describe the boundary surfaces of both the structure and the electrostatic field. The analysis electrostatic/structural domains are modeled by the nodes which are from the boundary grid and the background grid enclosed by the boundary surfaces. During the solution process, when the boundary surfaces of the structure move, those boundary nodes remain the same, while the internal nodes may be re-selected from the fixed background grid according to the new positions of the boundary surfaces. Hence, no matter how large the boundary surfaces deflect, regularly distributed internal nodes from the fixed background grid are obtained and the distortion of the analysis model is minimized. Therefore, the whole solution process can be automatically handled by the scheme proposed without the need of intervening, e.g. remeshing or rezoning. Several cases of electrostatic-structural coupled problems are tackled in this work to demonstrate the effectiveness and advantages of the novel meshless scheme.

Keywords: Electrostatic-structural analysis, background grid, meshless method, coupled-field analysis.

1 Introduction

One of the main disadvantages of the finite element method (FEM) to solve a problem is that it requires a mesh, including elements and nodes, and building the mesh is usually tedious and time-consuming. Although three-dimensional automatic mesh generators gradually become mature, they still are not popularly adopted

by the academia and industry since most of them can only generate tetrahedral elements instead of preferable hexahedral elements and create a large amount of elements, which become difficult to handle by computers and analysts.

In addition, the FEM usually gets troubles with the distortion of elements in dealing with large deformation problems. To overcome the distortion of elements, there exists a main idea which can partly solve the problems, i.e. to revise and improve the mesh quality adaptively during the solution process. The h-method, p-method and rezoning (remeshing the analysis domain) are some of the main tactics. But there are limits for the improvement by the h-method and p-method due to topology limitation, because the mesh adaptivity is based on the original mesh which may not suit the large deformation cases. As for rezoning, it still lacks an effective three-dimensional auto-rezoning program.

The meshless method has an inherent advantage that it doesn't require a mesh but a grid only, i.e. nodes' combination, and has become one of the most promising numerical methods. Based on the similar idea, there have been emerging some various meshless methods, such as, the element-free Galerkin method (EFGM)[Belytschko, Lu, and Gu (1994)], the reproducing kernel particle method (RKPM)[Liu, Jun, and Zhang (1995)], the $h-p$ clouds [Duarte and Oden (1996)], the node-by-node meshless method (NBNM)[Nagashima (2000)] and the meshless local Petrov-Galerkin method (MLPG)[Atluri and Zhu (1998); Atluri and Shen(2002); Atluri (2004); Atluri, Han, and Rajendran (2004); Atluri, Liu, and Han (2006)] etc. Although there were the pioneering successes by above works, in the early research works, most of the cases were two-dimensional problems. Till recent years, three-dimensional problems have also been successfully tackled [Chen and Guo (2001); Han and Atluri (2003); Li, Shen, Han and Atluri (2003); Han and Atluri (2004); Chen and Chen (2005); Chen and Lee (2005)]. Among these methods, the MLPG and EFGM are two of the most adopted ones. But, in solving large deformation problems, the severe change of the positions of nodes will cause an irregular grid and also induce serious numerical interpolation and integration problems with the meshless methods. That is, the quality of interpolation degrades when the grid is too coarse and the accuracy of integration deteriorates when the grid is too dense [Mukherejee, and Mukherjee, (1997)]. There are some proposed ways to handle these kinds of problems. Liu and Jun (1998), and, Hussler-Combe and Korn (1998) used the adaptivity of refining the region, similar to the h-method in the FEM, to improve the quality of the interpolation when the density of nodes is not dense enough. Jun and Im (2000) took the adaptivity of the density of background cells to improve the accuracy of the integration when the density of nodes is too dense. Duarte and Oden (1996), and, Liszka, Duarte, and Tworzydlo (1996) adopted the adaptivity of the degree of polynomials, similar to the p-method in the FEM, to

modify the accuracy of the interpolation. Combination of both above *h*- and *p*-methods also has been adopted.

Here, a more straightforward and easy-to-implement new meshless scheme is proposed for the analysis of three-dimensional large deformation coupled-field problems. By this scheme, a fixed regular background grid is devised [Chen, Chi, and Lee (2009)], of which the distribution and locations of nodes remain unchanged to cover the analysis domains during the solution process. The boundary surfaces of the analyzed domains are discretized as the boundary grid which is used to represent the deformable shape and positions of the analyzed domains. Namely, the analysis domain is modeled by the nodes of the deformable boundary grid and the nodes from the fixed background grid enclosed by the boundary surfaces, as the internal nodes. Actually, the contents of the internal nodes enclosed by the boundary grid from the background grid are changing adaptively according to the updated boundary surface' shape and position described by the boundary grid during the solution process. By this approach, proper nodes can be thus selected adaptively and regular distribution of the internal nodes can be kept. An effective computational scheme can be thus implemented easily with less numerical interpolation or integration problems.

In the EFGM and some other meshless methods, the domain integration is necessary. The Gaussian quadrature, of which the integration points selected are not uniformly distributed and weighted, is good for polynomial interpolation functions as in the FEM. But, it may induce some deviation of accuracy in the domain integration for those meshless methods whose interpolation functions are derived by the moving least square approximation. The main reason is that the positions of the Gaussian quadratures are no longer the best ones to sample the interpolation functions and the weighting values, which represent the volumes of the corresponding quadrature points, may improperly estimate the importance of those points. Especially when the integration volumes of certain quadrature points are across border, the improper estimations may induce nonignorable deviation. Hence, instead of Gaussian quadrature, a regular quadrature scheme is proposed here. In this way, every quadrature has the same weighting and is uniformly distributed. Moreover, the represented volumes of those quadrature points which cross border will be simply scaled by the ratio of the part inside the borders. By this way, the accuracy for integration can be improved. The comparison will be also demonstrated below.

To demonstrate the proposed meshless method, several electrostatic-structural analysis cases are selected and solved. They are electrostatically actuated MEMS components which are very common in MEMS applications. This kind of coupled-field analysis is a type of problem involving calculation of both electrostatic and structural physics. For example, a flexible electrode is attracted and largely deflected

by the force due to the electrostatic field. At the same time, the electrostatic field is also affected by the large deflection of the flexible electrode. It is necessary to re-mesh the electrostatic field by the FEM to avoid the serious distortion of the elements, which are altered seriously during the solution. Even by the meshless methods, as mentioned above, the irregular distribution of nodes also causes numerical problems. The advantage of the present meshless scheme is distinct for solving this kind of problem. For comparison purpose, the FEM solutions are also shown.

In addition to the cases analyzed here, since it can easily handle the interaction between the two corresponding fields, the new scheme can also be applied to other kinds of coupled-field large deformation problems, such as fluid-structural coupled problems, etc. Besides, although only the EFGM is used as a meshless platform here, the new scheme can be also implemented in other kind of meshless methods, such as the MLPG.

2 Moving least square approximation

In the MLPG, EFGM and some other meshless methods, the shape functions are derived by a moving least square approximation. That is, the value of field variable at any point can be predicted with the derived shape functions and the values of the nodes surrounding the discussed point.

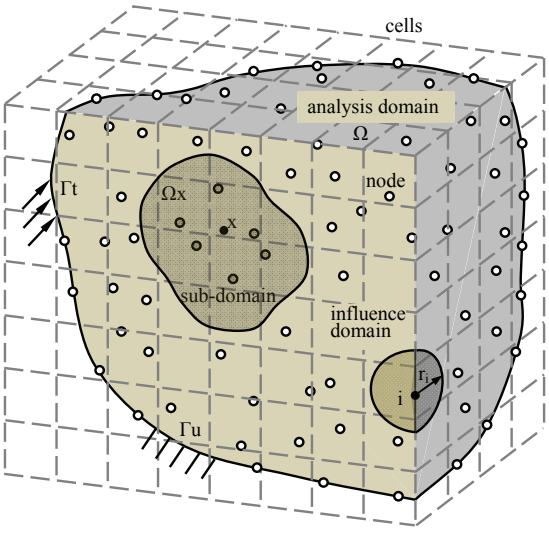

Figure 1: Meshless method

As shown in Fig.1, consider a sub-domain $\Omega\mathbf{x}$, which influences the node located at $\mathbf{x}$ inside the analysis domain Ω. The unknown field variable u can be expressed by an approximation function as u^h, say,

$$u^h = \sum_{j=1}^{m} p_j(\mathbf{x}) a_j(\mathbf{x}) = \mathbf{p}^T(\mathbf{x})\mathbf{a}(\mathbf{x}) \text{ in } \Omega\mathbf{x}, \tag{1}$$

where $\mathbf{p}^T(\mathbf{x}) = [p_1(\mathbf{x}), p_2(\mathbf{x})...p_m(\mathbf{x})]_{1\times m}$ is a complete monomial basis of order m. **a(x)** are unknown coefficients which are functions of the spatial coordinates $\mathbf{x}$. The coefficients **a(x)** can be determined by minimizing a weighted discrete L_2 norm, which is defined as

$$J(\mathbf{x}) = \sum_{i=1}^{n} w_i(\mathbf{x})[\mathbf{p}^T(\mathbf{x}_i)\mathbf{a}(\mathbf{x}) - u_i]^2, \tag{2}$$

where $w_i(\mathbf{x}) = w(\mathbf{x}-\mathbf{x}_i)$, u_i, $\mathbf{x}_i$ are the weight functions, nodal values, and coordinates associated with node i, respectively. n is the number of nodes in the influence domain of the discussed point in the sub-domain $\Omega\mathbf{x}$. In this work, the following quartic spline function is adopted as the weight function [Belytschko, Lu, and Gu (1994)]:

$$w_i(\mathbf{x}) = \begin{cases} 1 - 6(\frac{d_i}{r_i})^2 + 8(\frac{d_i}{r_i})^3 - 3(\frac{d_i}{r_i})^4 & 0 \le d_i \le r_i \\ 0 & d_i \ge r_i \end{cases}, \tag{3}$$

where $d_i = |\mathbf{x}-\mathbf{x}_i|$ denotes the distance between the discussed point and node i. r_i is the radius of the influence domain.

The stationary condition of weighted discrete L_2 norm $J(\mathbf{x})$ with respect to the coefficients **a(x)** leads to the relation

$$\mathbf{A}(\mathbf{x})\mathbf{a}(\mathbf{x}) = \mathbf{C}(\mathbf{x})\hat{\mathbf{u}}, \tag{4}$$

where

$$\mathbf{A}(\mathbf{x}) = \mathbf{P}^T\mathbf{W}\mathbf{P}, \tag{5}$$

and

$$\mathbf{C}(\mathbf{x}) = \mathbf{P}^T\mathbf{W}. \tag{6}$$

In Eq. (4), $\hat{\mathbf{u}}$ is the nodal values and $\mathbf{P}$ is the matrix of the above $\mathbf{p}^T(\mathbf{x})$ with the nodal coordinates of those nodes in the subdomain $\Omega\mathbf{x}$, and $\mathbf{W}$ is the diagonal weighting matrix of $w_i(\mathbf{x})$. Then, the coefficients **a(x)** of Eq. (1) can be derived as

$$\mathbf{a(x)} = \mathbf{A(x)}^{-1}\mathbf{C(x)}\,\hat{\mathbf{u}}\,. \tag{7}$$

As in the FEM, u^h can also be expressed by the form with shape functions as

$$u^h = \sum_{j=1}^{n} N_j(\mathbf{x}) u_j = \mathbf{N}^T \hat{\mathbf{u}}, \tag{8}$$

Comparing with Eq. (1), the nodal shape functions $\mathbf{N}$ can thus be derived as

$$\mathbf{N}^T(\mathbf{x}) = \mathbf{p}^T(\mathbf{x})\mathbf{A}(\mathbf{x})^{-1}\mathbf{C}(\mathbf{x}). \tag{9}$$

After the shape functions $\mathbf{N}$ have been derived, the equilibrium equations for analysis problems can then be formed by either the variational formulation or the Galerkin method as used in the FEM. The detailed derivation of the shape functions $\mathbf{N}$ by the moving least square approximation can also be referred to Atluri and Zhu (1998), Chen and Guo (2001).

3 The new meshless scheme with background grid

As mentioned above, the proposed new scheme is mainly for handling large deformation problems. For a large deformation problem, the entire solution process is divided into a certain number of solution steps. At each solution step, the deformation of the analyzed object is small enough to capture the complex nonlinear behavior for reaching good accuracy of the solution. During the solution process, the analyzed object is deflecting, i.e. deformed and displaced, step by step. Namely, the analysis domain representing the analyzed object is changing and moving in space during the solution process.

With this scheme, a regular background grid which covers the entire analysis domain is paved first, as shown in Fig. 2. Inside this, a set of boundary nodes, i.e. the boundary grid on Γ, are employed to represent the boundary of the analysis domain Ω, i.e. the surface of the analyzed object. That is, the analysis model is a combination of the boundary grid and the background grid during the step-by-step solution.

For each step, the nodes of the boundary grid and those nodes from the background grid enclosed by the boundary form an analysis domain Ω temporarily for the solution. When the boundary grid moves due to the deformation and displacement from previous solution step, it will enclose new nodes from the background grid. Those new enclosed nodes with the nodes of the boundary grid form an updated analysis domain for next step solution. The solution will move on in the same way.

For example, as shown in Fig. 2(a), the nodes of boundary grid representing the boundary Γ and the dark nodes enclosed by the boundary grid are considered as

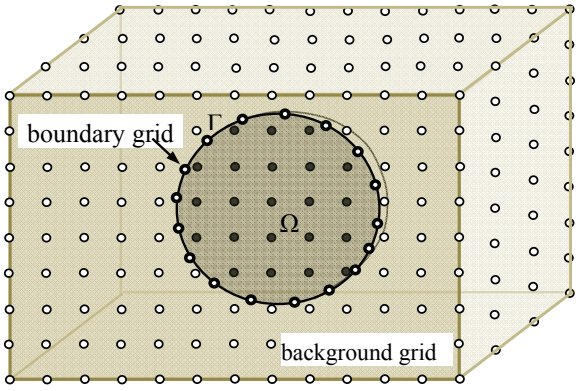

(a) original status

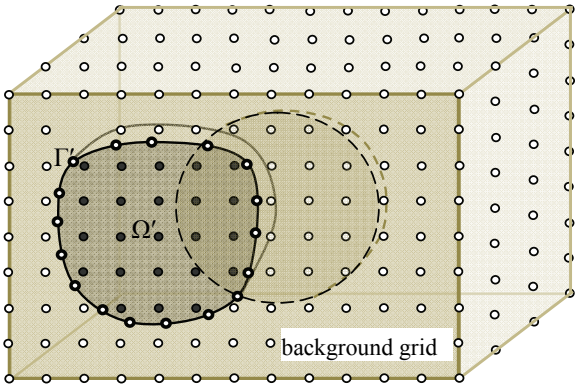

(b) deformed status

Figure 2: Model with background grid

active nodes and form the current analysis domain Ω for the first step solution. The nodes outside Γ are inactive and play no role at this solution step. The solution of this step is supposed to result in some deformation and displacement of the object, represented by the displaced boundary grid Γ', as shown in Fig. 2(b). At the next solution step, some originally-inside nodes will be left out of the Γ' and become ones of the inactive nodes, but some originally-outside inactive nodes will be newly enclosed by the boundary Γ' and become active as shown by dark nodes. All the active internal nodes with the nodes of the boundary grid form the new analysis domain, Ω'. After the new analysis domain has been determined, the solution for the new step is then being carried out accordingly. The process keeps going this way during the step-by-step solution.

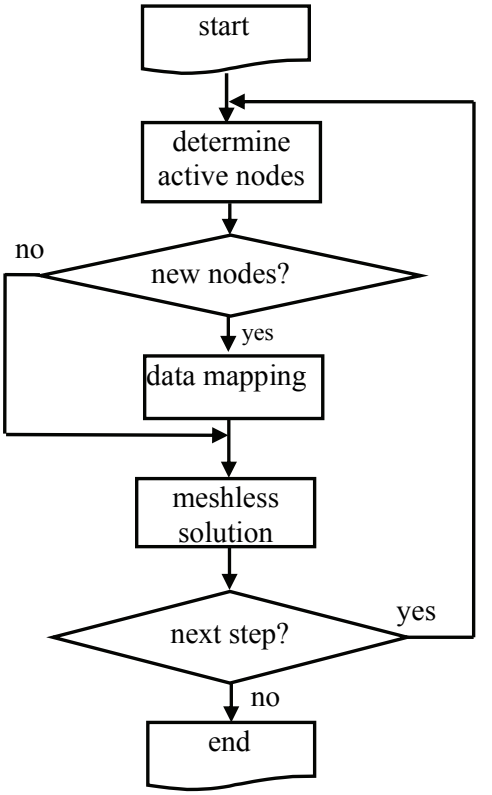

Figure 3: Flow chart of the new scheme with background grid for the meshless method

In this process, the active nodes of each solution step normally are different and adaptively coincide with the deformed and displaced objects. Because the background grid is fixed, although the active nodes are different, the regular nodal distribution of the analysis domain can be obviously kept. This is a distinct advantage of this scheme for numerical solution.

If the field variable results of the analysis are path independent, such as electric field in electrostatic problems which involves no time and history effect, no solution mapping, i.e. mapping the values of the old nodes onto the new nodes, is required. On the other hand, if the field variable results of the analysis are path dependent, such as stresses and strains of a material in nonlinear structural problems, variable value mapping is required. The procedure of the new scheme is illustrated in Fig. 3.

For coupled-field problems, e.g. electrostatic-structural cases, two analysis domain are needed for electrostatic and structural analysis respectively. When doing the structural analysis, the nodes inside the structure are to be selected for the structural solution. However, when doing the electrostatic analysis, the nodes outside the structure but inside the outer space boundary are to be selected for the electrostatic solution.

4 Governing equations for structural and electrostatic analyses

For the static structural analysis, the displacements, strains and stresses in structures subjected to external loads are to be determined. As shown in Fig.1, a three-dimensional structure Ω enclosed by a boundary is solved. The governing equation in static equilibrium condition is:

$$\nabla \cdot \boldsymbol{\sigma} + \mathbf{b} = 0 \qquad \text{in } \Omega, \tag{10}$$

where $\boldsymbol{\sigma}$ is the stress tensor and $\mathbf{b}$ is the body force vector. The corresponding boundary conditions are:

$$\boldsymbol{\sigma} \cdot \mathbf{n} = \bar{\mathbf{t}} \quad \text{on } \Gamma t \tag{11}$$

$$\mathbf{u} = \bar{\mathbf{u}} \quad \text{on } \Gamma u, \tag{12}$$

where $\bar{\mathbf{t}}$ is the prescribed traction acting on the traction boundary Γt and $\mathbf{n}$ is the outward unit normal vector to the boundary. $\bar{\mathbf{u}}$ is the prescribed displacement on the displacement boundary Γu.

For the electrostatic field analysis, the electric field and electric scalar potential distribution caused by applied potential or charge distributions are to be determined. The governing equation is

$$\nabla \cdot (\varepsilon \nabla \phi) = \rho, \tag{13}$$

where ϕ is the electric scalar potential and ρ is the volume charge density. ε is the permittivity of free space. The electric field intensity $\mathbf{E}$ can be derived by

$$\mathbf{E} = -\nabla \phi. \tag{14}$$

The attraction force calculated at certain point in the center of the corresponding area by the electric field intensity is derived by

$$f_n = 1/2 \varepsilon E_n^2, \tag{15}$$

where E_n is the electric field intensity in the direction normal to the surface area and f_n is the electric attraction force per unit area, namely normal pressure. The attraction force will be treated as the prescribed traction in the structural analysis, i.e. apply normal pressures which values are derived by eq. (15) on the corresponding areas of the surfaces of the electrode structure and do the structural analysis.

In electrostatic-structural problems, the structure is attracted to deflect by the electrostatic forces. At the same time, the deflected structure, which is also an electrode in the problem, causes the change of electrostatic field domain. Namely, the analysis domain of electrostatic field is changing during the solution process. Due to the two way effects between the electrostatic and structural field, a coupled-field analysis is needed to handle this kind of problem. In the present electrostatic-structural analysis, a sequential coupled analysis procedure is employed. That is, electrostatic field analysis and structural analyses will be done in turn, as shown in Fig. 4.

Based on the new scheme mentioned above, both physical domains use different portion of the same background grid and share the same boundary grid without re-zoning the analysis model during the solution process even in large deformation situations. Only the nodes for each solution step are adaptively selected in accordance with the "moving" boundary, i.e. the surfaces of the deflected electrode. In addition, the interaction between two physical domains can be automatically transferred through the same boundary grid shared by both sides. Thus, the whole solution process can be automatically handled by a program without any intervening modeling works, e.g. remeshing, which are required for severely distorted analysis domain in other numerical methods. Therefore, the efficiency of the new scheme becomes more distinct in this kind of coupled-field analysis problem.

The iterative procedure is shown in Fig. 4: (1) analyze the electrostatic field and calculate the attraction force due to the electric field intensity, (2) apply that attraction force on the structure and do the structural analysis to determine its deflection, and (3) the electric field is re-calculated according to the newly updated domain. Repeat steps (1) to (3) until the deviation of the deflections between two iterations, d_{n-1} and d_n, is small enough, i.e. $|d_n - d_{n-1}|/d_n$ is within acceptable tolerance.

5 The quadrature scheme for domain integration

For the integrals in the weak forms of equilibrium, i.e. volume domain integration, discrete analogs are adopted in numerical methods. For the EFGM, Belytschko et al. (1994) had proposed a way based on cell integration. In this way, the domain integration is similar to the element integration in the finite element method. The cells are in place of elements for the volume integration. In cell integration, a regular cell structure was also proposed, which is independent of the nodes and

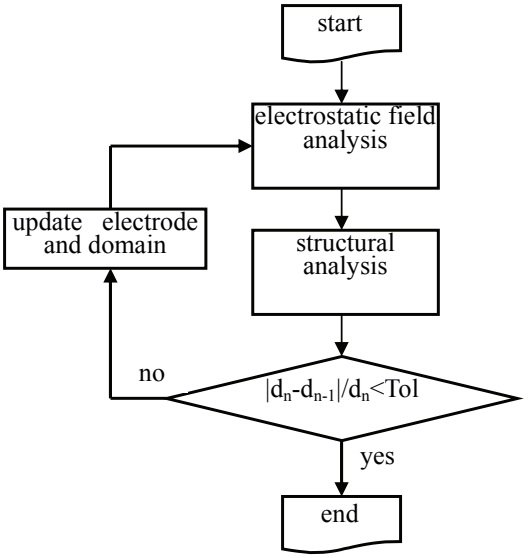

Figure 4: Flow chart for electrostatic-structural analysis

the boundary. Therefore, some cells may cross the boundary. A three-dimensional cell is a regular cube, in which some integration points are selected as the sample points which represent associated portions of the cell for numerical integration to get the integrals in the cell. If the cell is partially inside the domain, those integration points inside the domain will be taken into the integral and others will be neglected. In the EFGM and some other meshless methods, the Gaussian quadrature, which is not uniformly distributed and weighted, is used for domain integration. The Gaussian quadrature has been proved to be able to accurately represent the polynomial function in numerical integration and it is therefore adopted for the finite element method. But, the interpolation functions for those meshless methods, derived by the moving least square approximation as described above, are no longer polynomials. In addition, the moving least square interpolants are moving and randomly influenced by neighbor nodes, the values of field variable inside the cell are so irregular such that the Gaussian quadrature cannot be considered as the always-good sampling way. The positions of the quadrature may not be the best position to sample the interpolation functions. The weighting value which represents the volumes of those positions may improperly estimate the importance of those positions especially when the integration volumes of certain quadrature points are across the boundary. Instead of Gaussian quadrature, a regular quadrature is thus proposed here. Every quadrature has the same weighting and is uniformly dis-

tributed. Therefore, when encountering the boundary mismatching situation, i.e. the boundary of the analysis domain doesn't coincide with the cells' boundaries as seen in Fig. 5, the deviation of accuracy will be statistically reduced due to equal weighting. In addition, in this scheme, the represented volumes of those quadrature points which cross the boundary will be simply scaled down by the ratio of the part inside the domain. By this way, the accuracy for integration can be improved and the comparison will be also demonstrated below.

6 Numerical examples

For evaluating the performance of those two different types of quadrature mentioned above, a cantilever beam, 1μm x 1μm x 10μm, subjected to bending and stretching, as shown in Fig. 6, was analyzed. The Young's modulus is 50,000 MPa and the Poisson's ratio is 0.17. The values of the loads are 1 μN. In this example, analyses with different cell sizes were conducted to simulate various situations that may be encountered during different solution processes. Sometimes the boundary of the analysis domain coincides with the cells' boundaries; sometimes it doesn't, as shown in Fig. 5 schematically. The deviation comparisons between the Gaussian and uniform quadrature for two load types versus the cell size are shown in Fig. 7 and 8, respectively. For comparison purpose, the exact solutions of the largest displacements for both two load types are normalized to unity. It is found that both type of quadrature can obtain good results when the boundary of the analysis domain coincides with the cells' boundaries. But if they don't coincide with each other, the inaccuracy of the results by the Gaussian quadrature is much higher than those by the uniform quadrature, e.g. when the cell size is 0.3μm.

To demonstrate the procedure and effectiveness of the new meshless scheme, two electrostatic-structural analysis cases are carried out then. For comparison purposes, the FEM will also be employed to solve the same problems.

The structure in the first case is a pair of electrode beams as shown in Fig. 9. The top electrode beam is cantilevered and actuated by the grounded bottom electrode beam due to the voltage drop. A zero voltage is applied to the bottom electrode. A nonzero voltage is applied to the top electrode. The voltage difference of 120 volts produces electrostatic force on the top electrode and causes it to deflect toward the bottom electrode. The attraction force and equilibrium position is going to be determined. A moderate size of free space is adopted for electric field analysis. The Young's modulus of the electrode beams, a kind of Oxide, is 50,000 MPa. The Poisson's ratio is 0.17. The beam's size is 0.4μm x 0.2μm x 5μm. The gap between the two beams is 1.0 μm. The ANSYS® program was also used to solve the same case. But, the solution always breaks down due to the severe distortion of the mesh no matter how fine the mesh is as schematically shown in Fig. 10. It is necessary

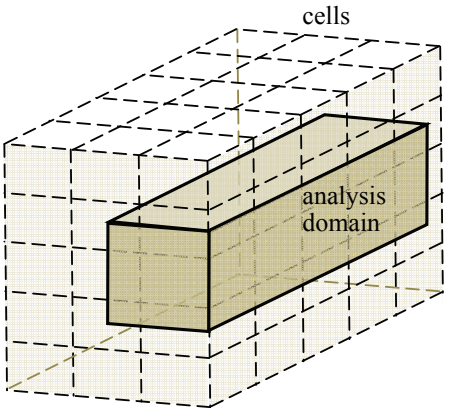

Figure 5: Relationship between the integration cells and analysis domain

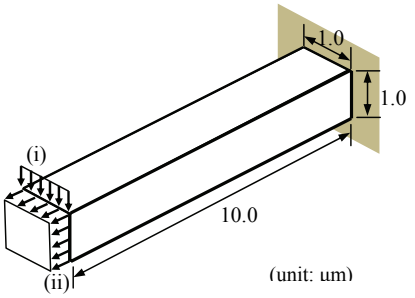

Figure 6: A cantilever beam subjected to: (i) bending, and (ii) stretching

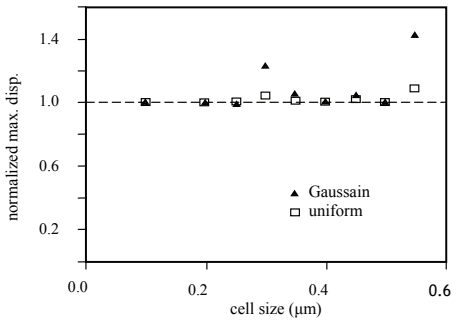

Figure 7: The deviation comparison between the Gaussian and uniform quadrature versus cell size for bending case

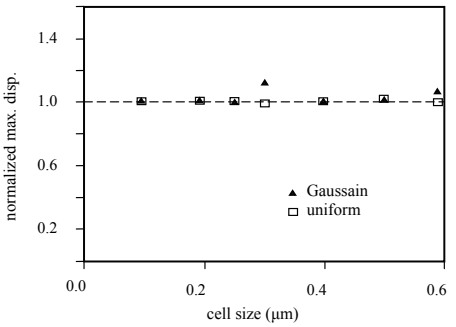

Figure 8: The deviation comparison between the Gaussian and uniform quadrature versus cell size for stretching case

to re-mesh the electric field domain to make the solution properly works. Because the auto-mesher can only generate tetrahedral elements, a tetrahedral element type for re-meshing is adopted in this work. When using the meshless method without background grid, it is noted that the nodes for electrostatic analysis will pierce into the structure domain when the structure deflects and won't be able to continue the solution process. The meshless model with background grid is shown in Fig. 11.

The attraction force and the displacement at the tip of the top beam electrode are shown in Table 1, respectively. It is obvious that, if the influence of the deflection

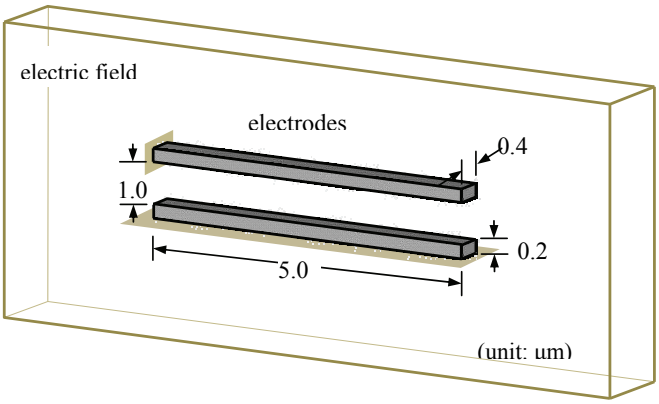

Figure 9: Electrostatic-structural analysis for two electrodes in electric field

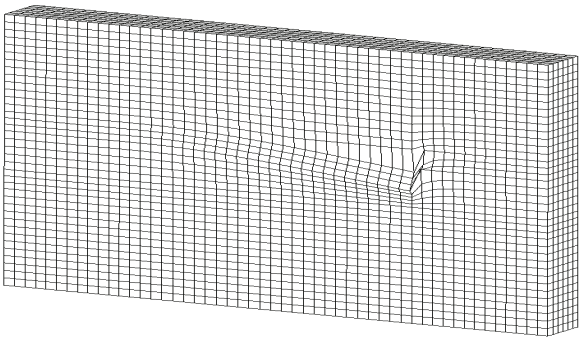

Figure 10: Element distortion by finite element analysis

of the top beam electrode on the attraction force is neglected and simply the attraction force computed from the original position is used, there will be a significant inaccuracy involved in.

The second case is a silicon microphone [Miao, Lin, Chen, Zou, Lim, and Seah (2002)] whose basic structure is shown in Fig. 12. Here, due to symmetry, it is sufficient to solve a quadrant of the problem. A diaphragm and a perforated backplate form a pair of capacitor. It is a kind of transducer that converts sound into electrical signals. The mechanism is that the sound pressure will induce the deflection of the diaphragm and change the gap between the diaphragm and the backplate. The capacitance of the capacitor, which is a manipulable electrical signal, is then deter-

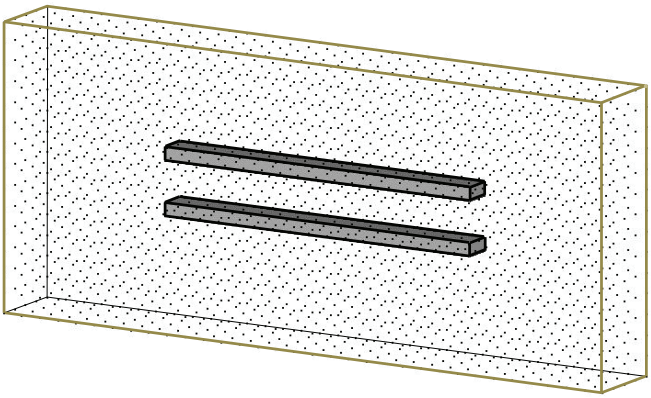

Figure 11: Electrostatic-structural analysis for two electrodes in electric field by meshless method with background grid

Table 1: The attraction force and the displacement at the tip

	attraction force in original position (μN)	attraction force in deflected position (μN)	Displacement (μm)
Proposed scheme (nodes: 5,658)	0.169	0.266	0.33
ANSYS® (elements: 3,689, nodes: 6,176 *)	0.179	0.250	0.35

For electrostatic analysis, the ANSYS® program only has second-order element types. For each second-order tetrahedral element, it contains 10 nodes.

mined. Thus, to know the acoustics characteristics of the silicon microphone, it is necessary to check the displacement versus applied voltage during the design stage. In this case, a coupled analysis was adopted to obtain the displacement over voltage drop. As shown in Fig. 12, the radius of the ventilation holes on the backplate is 10 μm. The size of the backplate is 400 μm x 400 μm, which is fixed along the edges. The diaphragm beneath is H-shaped. The ends of the legs of "H" are fixed. The thicknesses of the backplate and diaphragm are 5 μm and 3 μm, respectively.

The elastic modulus of the silicon diaphragm is 120 GPa; the Poisson's ratio is 0.22. The voltage drop is applied to the pair of capacitor electrodes, diaphragm and backplate, from 1 to 4 volts, respectively. The voltage difference produces

electrostatic force on the diaphragm and causes it to move toward the backplate to reduce the gap. The equilibrium position can then be determined. A moderate size of free space is adopted for the electric field analysis. The ANSYS® program is also employed to solve the same case. When doing these analyses, the difficult situations for the ANSYS® program and the meshless scheme without background grid encountered in the previous case still remain.

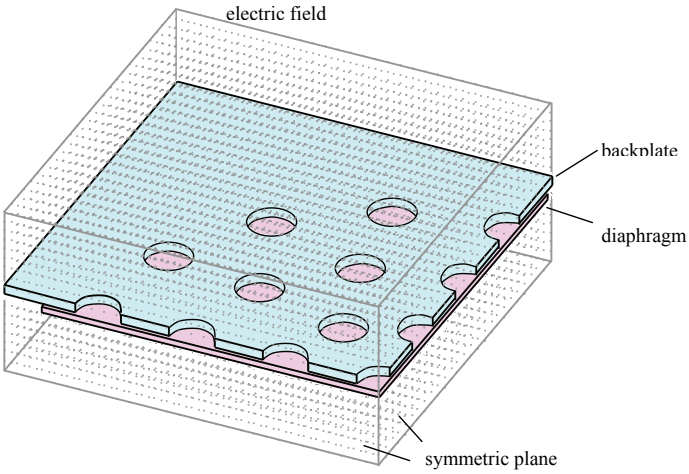

Figure 12: Electrostatic-structural analysis for a microphone by meshless method with background grid

The results of the displacement at the center of the diaphragm versus different voltage drop are displayed in Fig. 13. The results from the ANSYS® program are almost the same even when decreasing the element size by a half. And the results obtained by the two methods are also rather consistent as the figure demonstrates.

7 Conclusions

In dealing with electrostatic-structural problems, extremely large deformation and coupled effect are the two important and difficult issues to be tackled. By those two electrostatic-structural examples demonstrated above, they show that the coupled effect cannot be ignored. In addition, the simulation difficulties due to coupled effect and large deformation can be easily and efficiently handled by the proposed new meshless scheme with background grid.

This scheme is quite straightforward and efficient even for coupled-field problems

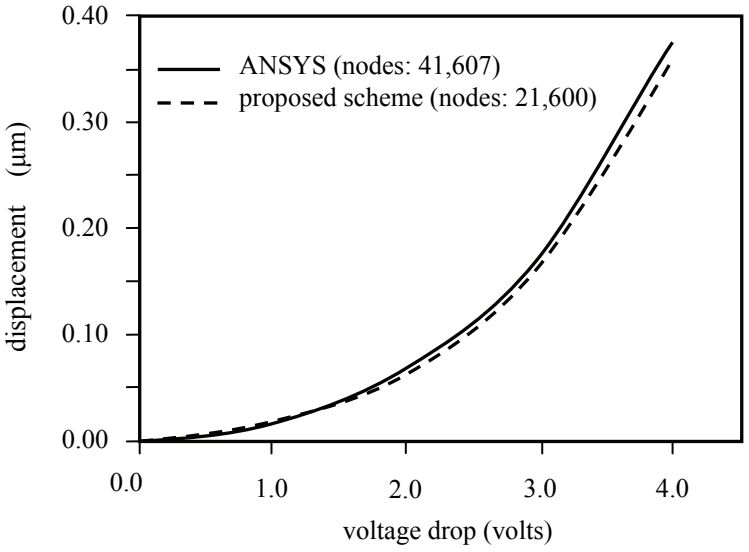

Figure 13: Displacements at the center of the diaphragm versus voltage drop

with severe large deformation. In addition to the electrostatic-structural problems, the way to implement the new scheme can also be applied, in the future, to other types of coupled-field problems with large deformation, e.g. fluid-structural coupled problems in which the flow pressure will induce the structure's deflection which may cause the change of the flow pattern.

The accuracy issue with the numerical integration over the analysis domain is frequently encountered for meshless methods due to the boundaries of the analysis domain and the integration cells may not coincide. In many cases, it requires to increase the number of the quadrature points to obtain better accuracy at the price of more computing time. In this works, the proposed uniform quadrature scheme has been proved to be able to handle the numerical integration more accurately. It means that the uniform quadrature scheme can reach the same level of solution accuracy with less quadrature points. It is also mentioned that the proposed schemes can also be implemented with most kinds of meshless methods in a similar way, such as the MLPG, etc.

References

Atluri, S. N.; Zhu, T. (1998): A new meshless local Petrov-Galerkin (MLPG) approach in computational mechanics. *Comput. Mech.*, vol. 22, pp. 117–127.

Atluri, S. N.; Shen. S. (2002): The Meshless Local Petrov-Galerkin (MLPG) Method: A Simple & Less-costly Alternative to the Finite Element and Boundary Element Methods. *Comput. Mech.*, vol. 3, no. 1, pp. 11-52.

Atluri, S. N. (2004) : The Meshless Method (MLPG) for Domain & BIE Discretizations, 680 pages, *Tech Science Press.*

Atluri, S. N.; Han, Z. D.; Rajendran, A. M. (2004) : A New Implementation of the Meshless Finite Volume Method, Through the MLPG "Mixed" Approach,*CMES: Computer Modeling in Engineering & Sciences*, Vol. 6, no. 6, pp. 491-513.

Atluri, S. N.; Liu, H. T.; Han, Z. D. (2006) : Meshless Local Petrov-Galerkin (MLPG) Mixed Collocation Method For Elasticity Problems,*CMES: Computer Modeling in Engineering & Sciences*, Vol. 14, no.3, pp. 507-518.

Belytschko, T.; Lu, Y.Y.; Gu, L. (1994): Element-Free Galerkin Method. *International Journal for Numerical Methods in Engineering,* vol. 37, pp. 229-256.

Chen, W. H.; Guo, X. M. (2001): Element Free Galerkin Method for Three-dimensional Structural Analysis, *CMES: Computer Modeling in Engineering & Sciences,* Vol. 2, no. 4, pp. 497-508.

Chen, W. H.; Chen, C. H. (2005): On Three-Dimensional Fracture Mechanics Analysis by an Enriched Meshless Method, *CMES: Computer Modeling in Engineering & Sciences*, Vol. 8, no. 3, pp. 177-190.

Chen, W. H.; Lee, M. H. (2005): On Three-Dimensional Electrostatical- structural Analysis Using Galerkin Meshless Method, *The 29th National Conference on Theoretical and Applied Mechanics*, Hsinchu, Taiwan, R.O.C., 16-17 Dec., 2005.

Chen W.H.; Chi C.T.; Lee M.H. (2009): A Novel Element-Free Galerkin Method with Uniform Background Grid for Extremely Deformed Problems, *CMES: Computer Modeling in Engineering & Sciences,* Vol.40, No.2, pp. 175-200.

Duarte, C. A.; Oden, J. T. (1996): An h-p adaptive method using clouds. *Computer Methods in Applied Mechanics and Engineering,* vol. 139, pp.237-262.

Han, Z. D.; Atluri, S. N. (2003) : Truly Meshless Local Petrov-Galerkin (MLPG) Solutions of Traction & Displacement BIEs, *CMES: Computer Modeling in Engineering & Sciences*, Vol. 4, no. 6, pp. 665-678.

Han, Z. D.; Atluri, S. N. (2004): Meshless Local Petrov-Galerkin (MLPG) approaches for solving 3D Problems in elasto-statics, *CMES: Computer Modeling in Engineering & Sciences*, Vol. 6, no. 2, pp. 169-188.

Hussler-Combe, U. Korn, C. (1998): An adaptive approach with the element-free Galerkin method. *Computer Methods in Applied Mechanics and Engineering,* Vol. 162, 1998, pp.203-222.

Jun, S.; Im, S. (2000): Multiple-scale meshfree adaptivity for the simulation of adiabatic shear band formation. *Computational Mechanics* vol. 25, pp.257-266.

Li, Q.; Shen, S.; Han, Z. D.; Atluri, S. N. (2003) : Application of Meshless Local Petrov-Galerkin (MLPG) to Problems with Singularities, and Material Discontinuities, in 3-D Elasticity, *CMES: Computer Modeling in Engineering & Sciences*, Vol. 4, no. 5, pp. 567-581.

Liszka, T.J.; Duarte, C.A.M.; Tworzydlo, W.W. (1996): hp-Meshless cloud method. *CMES: Computer Modeling in Engineering & Sciences*, vol. 139, pp.263-288.

Liu, W. K., Jun, S. and Zhang, Y. F. (1995) : Reproduction Kernel Particle methods, *International Journal for Numerical Methods in Fluids*, Vol. 20, pp. 1081-1106.

Liu, W. K.; Jun, S. (1998): Multiple-scale reproducing kernel particle methods for large deformation problems. *International Journal for Numerical Methods in Engineering,* vol. 41, pp. 1339-1362.

Miao, J.; Lin, R.; Chen, L.; Zou, Q.; Lim, S.Y.; Seah, S.H. (2002): Design considerations in micromachined silicon microphones. *Microelectronics Journal,* vol.33, pp.21-28.

Mukherejee, Y. X.; Mukherjee, S. (1997): On boundary conditions in the element free Galerkin method. *Computational Mechanics* vol.19, pp.264-270.

Nagashima, T. (2000): Development of a CAE system based on the node-by-node meshless method, *CMES: Computer Modeling in Engineering & Sciences*, Vol. 187, pp.1-34.